NDT&E International 158 (2026) 103576

Contents lists available at ScienceDirect

NDT and E International

journal homepage: www.elsevier.com/locate/ndteint

Ultrasonic imaging using a phased array probe with a buffer consisting of a bundle of circular cylinders

Mingqian Xia, Kohei Nishiuchi, Takahiro Hayashi *, Naoki Mori

Graduate School of Engineering, The University of Osaka, Japan

A B S T R A C T

The authors have previously investigated defect imaging using a phased array probe with a buffer consisting of thin plates. Although the phased array probe with a stacked plate buffer works well in defect imaging, there remains the issue of spurious images due to trailing waves generating at the side walls of a plate, and large stacked plate buffers are required to avoid the trailing waves. To solve these issues, a buffer consisting of circular cylinders is introduced. Considering dispersion characteristics of longitudinal vibration mode of guided waves in a circular cylinder and dimensions of phased array probe, cylinder buffers were designed and fabricated. Using the buffer consisting of circular cylinders, defects were well visualized with two imaging algorithms, plane wave imaging and total focusing method.

1. Introduction

Inspection techniques including visual checking for working plants, ultrasonic and radiographic inspections are required for regular health monitoring for all industrial plants, including nuclear power plants, steel mills and chemical plants for guarantee the work safety. Particularly, pipes are often experiencing stress corrosion cracking (SCC) and fatigue cracking due to the content and pressure changing inside pipes [1–6]. Since pipe collapse caused by SCC and fatigue cracks often happen in heat-affected zones (HAZs) near welds in pipes, inspecting HAZs in pipeworks is a key technology to locate the cracks precisely and to make sure the remaining service life in working environment [7–16].

Phased array ultrasonic testing (PAUT) have been widely used recently for such pipe weld inspection, in which many equally spaced piezoelectric elements transmit and receive ultrasonic signals, and the ultrasonic signals are processed into defect images through imaging algorithms. Many data acquisition methods in the phased array (PA) imaging such as sectorial scanning, full matrix capture, plane wave imaging, and imaging methods such as total focusing method, delay-and-sum, synthetic aperture focusing, are widely used in practical testing [17–22]. In this study, Plane Wave Imaging (PWI) and Full Matrix Capture/Total Focusing Method (FMC/TFM) are used in experiments. The PWI simultaneously excites signals from N array elements to the specimen to be tested, then the $1 \times N$ signals received at the N array elements are processed for defect image. In FMC/TFM, $N \times N$ signals are acquired by switching the incident array element and receiving with N array elements in one signal emitting and receiving period, and a defect image is generated based on the $N \times N$ signals.

Although the PAUT has become a standard technique for nondestructive inspection in plants, there are still challenges when considering harsh environment of working pipelines. Normally in the PAUT, the PA probe has to be in contact with the object to be inspected, but this is not possible if the temperature of object is high or low enough to damage the PA probe. For example, liquid sodium has been a type of liquid coolant for some newly built nuclear power plants, where the temperature of the pipeline system that transports the coolant is around 500 °C. At the same time, the PA probe often needs to be kept at no more than adhesive endurance temperature, e. g., 60 °C, to maintain normal operation. A bulk buffer rod can be a solution for ultrasonic testing in such high temperature, by cooling with coolants such as water and air, emitting ultrasonic waves, and keeping the contact area with the ultrasonic probe within a tolerable temperature range. However, a bulk buffer rod can be used as a solution for a single ultrasonic probe, which cannot be applied for PA probes because the image cannot be obtained due to the near field limit [23–25].

In our previous studies, a stacked plate structure was considered instead of a bulk buffer rod as a solution for the PA imaging with a buffer. Fukuchi. et al. numerically investigated the ultrasonic focusing by a stacked plate structure and revealed that ultrasonic focusing is possible by stacked thin plate structure beyond the near field limit [26]. Based on the numerical analyses and experimental investigations of the wave propagation in the stacked plate structure, the authors of the current paper confirmed that the defect imaging with a PA probe with a stacked plate buffer works well [27,28]. However, spurious images were also observed in the images, and our previous paper about the experimental investigation of feasibility of stacked plate buffer proved that

* Corresponding author.
E-mail address: hayashi@mech.eng.osaka-u.ac.jp (T. Hayashi).

https://doi.org/10.1016/j.ndteint.2025.103576
Received 4 August 2025; Received in revised form 16 September 2025; Accepted 7 October 2025
Available online 8 October 2025

they are caused by the trailing waves generating at the side walls of the plate with finite width [28]. To eliminate the spurious images caused by the trailing waves, our previous study proposed the use of wider plates of the buffer. Although the solution successfully removes the spurious images, it necessitated the use of large buffer plates, which often hinders inspection personnels in the limited space of inspection sites. In this paper, a thin circular cylinder is proposed as a waveguide to solve these issues.

The purpose of this research is to experimentally confirm the feasibility of PA imaging using a probe with a buffer consisting of a bundle of circular cylinders. As a fundamental investigation, we first conduct an experimental study at room temperature. In Section 2, the principle of the PA imaging using a buffer consisting of a bundle of circular cylinders is explained. Section 3 describes the experimental devices and methods, including the PA probe, specimen, buffer, and imaging algorithms used in the experiments. In Section 4, the results of experiments with different length buffers are provided.

2. Use of circular cylinder bundle for a phased array buffer

Our previous studies proved using numerical simulations and experiments that PA defect imaging is feasible when a buffer consisting of a bundle of thin flat plates is attached to a PA probe. All waves propagating in plates maintain their waveforms and time delays due to small dispersion characteristic of S0 mode of Lamb waves in low frequency-thickness product range, and therefore the stacked-plate buffer can extend the imaging range compared to the bulk buffer rod. However, these studies showed that there are two limitations to the use of the stacked-plate buffer. One is the limitation of imaging area due to multiple reflections at both ends of the buffer [27], and the other is generation of spurious images due to trailing waves caused by mode converted waves at both side walls of the plates [28]. Although the first limitation is inevitable as long as buffers are used for phased array imaging, the second one about trailing wave was solved in the previous study by expanding the width of the buffer plate. However, the use of larger buffer may pose problems in inspection sites, considering that many inspection areas do not have sufficient space.

In this paper, an alternative way to solve the issue of trailing waves is proposed by using circular cylinders. The method of eliminating trailing waves from the waveguide can be explained qualitatively from the theory of generation of trailing waves and more precisely from the theory of propagation of guided waves in a circular cylinder, as follows.

Trailing waves in a flat plate with finite width are generated by mode conversion that occurred at the side walls of the plate. An S0 mode of Lamb wave propagates in a plate and the spread wave reflects at the side walls, causing some mode conversion, resulting in shear horizontal waves. In such case, due to differences in the propagation distance and propagation speed, it is known that even if a single longitudinal pulse wave is incident on the end of the buffer, multiple trailing waves are observed on the opposite side of the buffer with a certain time interval following the incident main straight wave pocket [28,29].

In the previous study of stacked plate buffer, we analyzed the trailing wave for an isotropic thin plate with a finite width under the assumption of plane stress condition. When the plate width of the buffer is w, the wave velocity of the S0 mode and the transverse wave velocity in the thin plate are c_{plate} and c_T, respectively, and the reflection angle when the mode conversion from the S0 mode to the SH wave occurs is α, the interval of multiple trailing waves, Δt_{plate}, can be expressed as

$$\Delta t_{plate} = \frac{w}{c_T \cos\alpha} - \frac{w}{c_{plate}} \tan\alpha, \tag{1}$$

Based on Eq. (1), increasing the width of the thin plate w leads to longer time interval Δt_{plate}, and resulting elimination of the influence of the trailing wave from the imaging area.

The interval of the trailing waves can be calculated in the same way for a circular cylinder. The interval after which the trailing wave appears, $\Delta t_{cylinder}$, can be expressed as

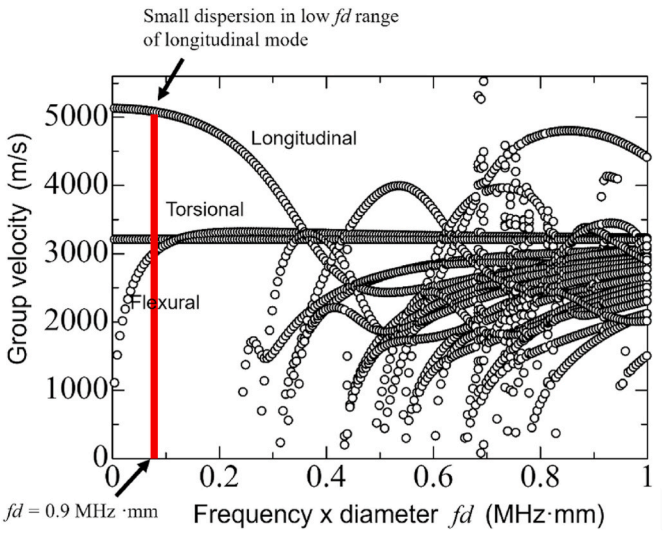

Fig. 1. Group velocity dispersion curves of guided waves for a circular cylinder with longitudinal and transverse wave velocities of 5790 m/s and 3100 m/s, respectively.

$$\Delta t_{cylinder} = \frac{d}{c_T \cos\beta} - \frac{d}{c_L} \tan\beta, \tag{2}$$

where d is the diameter of the circular cylinder, c_L and c_T, are the longitudinal wave velocity and the transverse wave velocity in the circular cylinder, respectively, and β is the reflection angle when the mode conversion from longitudinal wave to transverse wave occurs at the cylinder side wall [29].

Therefore, as with the thin plate, by increasing the diameter of the circular cylinder and delaying the arrival time of the trailing wave, it may be possible to eliminate its influence outside the imaging area. However, circular cylinders with a large diameter cannot be used as the PA buffer because the contact area to the PA probe becomes larger than the width of the single element of the linear array PA probe. Conversely, by reducing the diameter of the circular cylinder and shortening the interval of the trailing wave, it may be possible to concentrate the trailing waves closed to the main straight wave pocket, which will be used in this study.

To accurately analyze wave propagation in a circular cylinder, the wave field must be considered as guided waves. Fig. 1 shows the group velocity dispersion curves for a stainless-steel circular cylinder with longitudinal wave velocity 5790 m/s, transverse wave velocity 3100 m/s, used in later experiments. The dispersion curves were obtained by the semi-analytical finite element method [30]. The horizontal axis is the product of frequency (f) and diameter(d) of a circular cylinder, and the vertical axis is the group velocity (c_g). The mode with the largest group velocity represents the mode of longitudinal vibration, which can be generated by excitation in the axial direction from the cross-section of the circular cylinder. The longitudinal vibration mode has low dispersion in the low fd range and can be used as buffers in the same way as thin plates [27,28]. Namely, pulse wave generated at the one end of a circular cylinder can reach the opposite end with nearly the same waveform. In the latter experiments, the fd range shown in the red band is used, and the group velocity obtained by the calculation is 5060 m/s. Theoretically, it may be possible to use square cylinders and cylinders with an arbitrary cross-section as well as circular cylinders, but due to its availability, circular cylinders are adopted as a buffer element in this study.

Considering the use of circular cylinders as a PA buffer, the configuration is as shown in Fig. 2. The pitch and diameter of a buffer

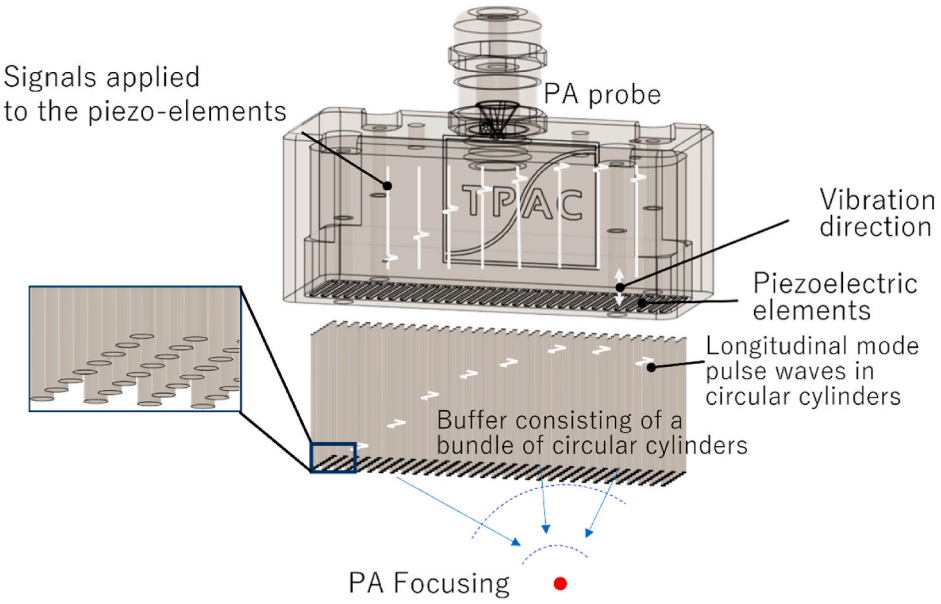

Fig. 2. Schematic diagram of phased array focusing with a buffer consisting of a bundle of circular cylinders.

consisting of a bundle of circular cylinders are adjusted so that each piezoelectric element of the PA probe corresponds to the end of a bundle of circular cylinders. Vibrations of the individual piezoelectric elements can propagate through each circular cylinder to the other end when the PA probe contacts with the end of the buffer consisting of a bundle of circular cylinders. In other words, the presence of the buffer can still transmit the vibrations from the PA probe and the object contact with the end of the buffer can be vibrated, as if the PA probe directly contact with the object. The nature of guided waves propagating through the circular cylinder is used.

The individual vibrating elements of the PA probe emit longitudinal waves with displacements perpendicular to the vibrating surface, so that vibrations in the longitudinal direction of the circular cylinders are incident on the edge surface of the circular cylinders. Because this vibration resembles the vibration distribution of the first longitudinal mode on the cross-section of the circular cylinder, most of the wave modes propagating in the circular cylinder are the first longitudinal mode.

When these ends are in contact with the object and delays are given to the elements in the PA probe as shown in Fig. 2, for example, the delays given by a PA probe and the ultrasonic pulses are almost unchanged at the other end. Thus, the ultrasonic PA technology can be used nearly without modification by using a buffer consisting of a bundle of thin circular cylinders.

3. Experimental equipment, buffer, and test specimen

This section describes the experimental equipment and test specimen used in the imaging experiment and fabrication of a buffer consisting of a bundle of circular cylinders.

A linear array PA probe consisting of 64 elements with an element size of 15 mm × 0.9 mm, a pitch of 1 mm, an element gap of 0.1 mm, and a total aperture of 15 mm × 63.9 mm is used in the experiments. The bandwidths of all elements are almost identical, with a center frequency of 1.0 MHz and a full width at half maximum of approximately 1.0 MHz. The experimental data were acquired by PWI and FMC using PA equipment (The Phased Array Company, Explorer). The system uses a 14-bit 64-channel architecture and can perform acquisition of all 64 channels in parallel at a sampling frequency of 50 MHz. In these experiments, the controller was driven by a PC using a LabVIEW interface. Each element of the PA probe can apply a longitudinal force at the edge

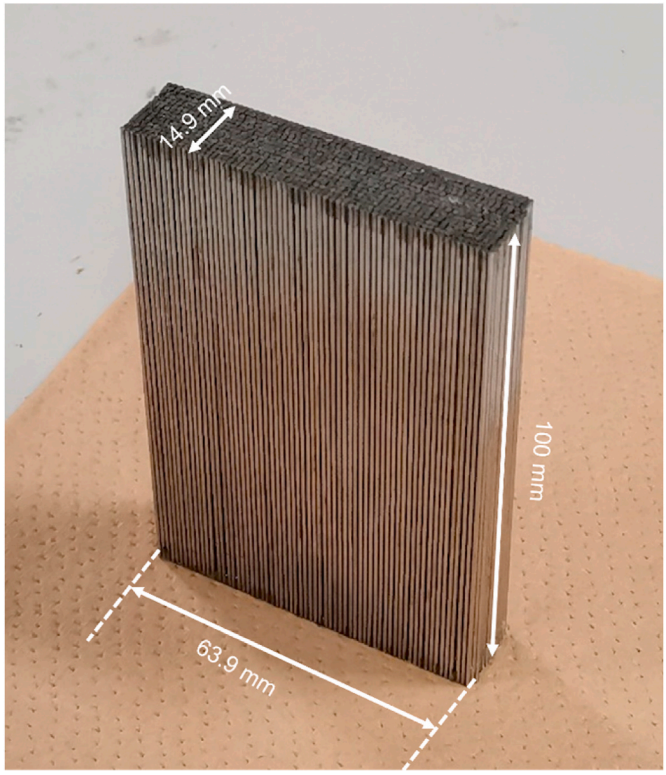

Fig. 3. Pictures of a buffer consisting of a bundle of circular cylinders has been formed by circular cylinders.

of each circular cylinder and inject an ultrasonic pulse wave with a center frequency of 1 MHz into each circular cylinder paired with each piezoelectric element.

Fig. 3 shows a picture of the buffer consisting of a bundle of circular cylinders used in the experiments in the next section. The SUS304 circular cylinder is with 0.9 mm diameter, which is the same as the width of the piezo element of the PA probe, and 100 mm long, which is the same length of the stacked plate buffer investigated by numerical calculations and experiments in the previous study. Fig. 4 shows the end surface of

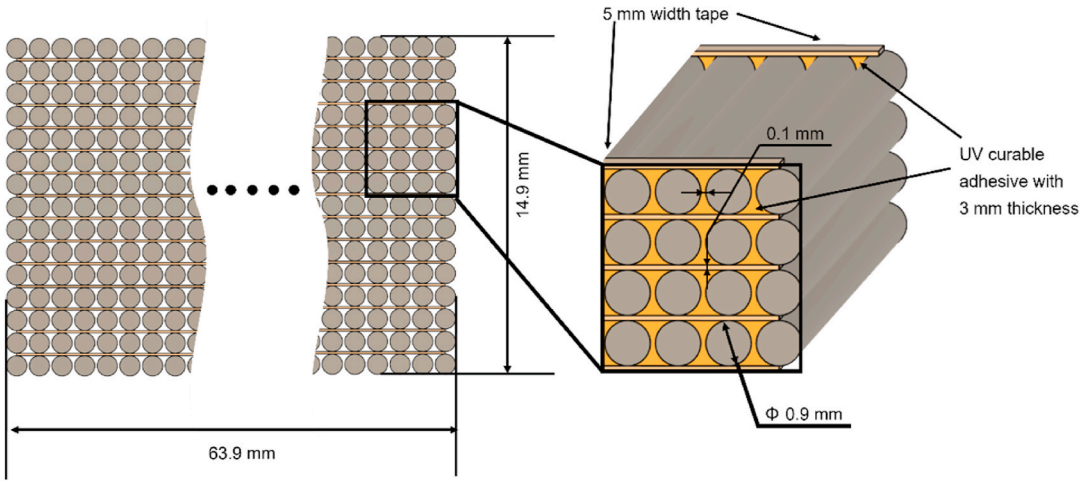

Fig. 4. Schematic diagram of the end surface of buffer consists of a bundle of circular cylinders.

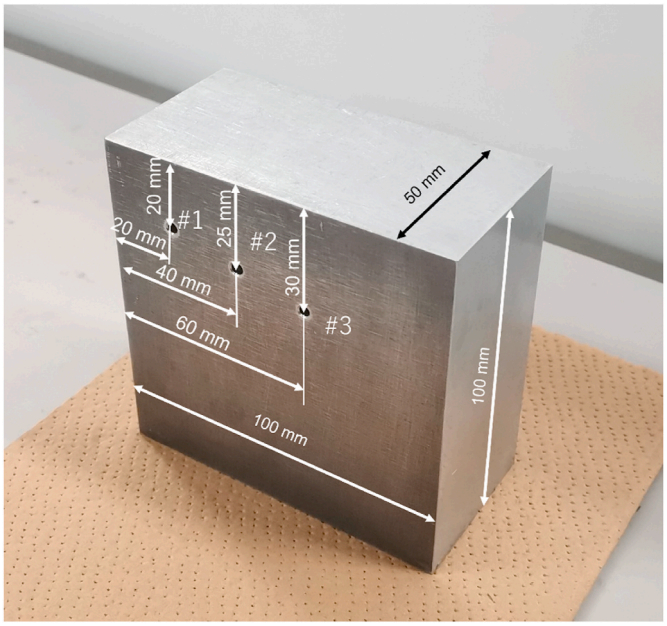

Fig. 5. A picture of the specimen with three side-drilled holes as internal reflectors to test the effectiveness of the buffer consisting of a bundle of circular cylinders.

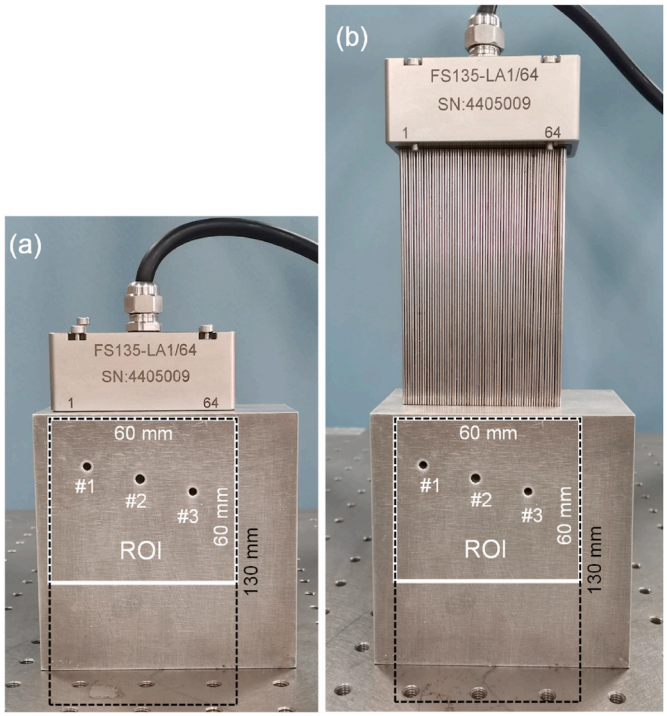

Fig. 6. Pictures of the experimental devices and specimen when (a) phased array probe without buffer, and (b) with the buffer consisting of a bundle of circular cylinders.

the buffer. 64 circular cylinders were arranged horizontally on a solid fixture with parallel notches of a 1 mm pitch, and the positions were fixed by curing the area about 3 mm from the ends of circular cylinders with a UV-curable adhesive which is shown in yellow between circular cylinders. The resulting gaps between the horizontally-arranged cylinders are 0.1 mm, and maintaining this gap is important for reducing crosstalk between each channel. Each layer consisting of 64 circular cylinders was then bonded with double-sided tape of 5 mm wide and about 0.1 mm thick. Stacking 15 layers created a cylinder-bundled buffer of about 15 mm wide. After that, to fix the buffer and to prevent the penetration of couplant, the gaps at both ends of the buffer were filled with UV-curable adhesive again. In this way, 15 circular cylinders arranged in a line can be paired with one piezoelectric element of the PA probe. Similarly, each piezoelectric element is paired with the other 15-cylinder row, as shown in Fig. 4.

Longitudinal wave with center frequency of 1 MHz from each piezoelectric element is applied on each circular cylinder and a longitudinally vibrating guided wave mode which has similar vibration form on the cylinder edges as the incident wave from piezoelectric elements, mainly propagates in the circular cylinders. Considering the dispersion curve of low *fd* range of 0.9 MHz mm, the longitudinal mode of guided wave can propagate in a very low dispersion.

As shown in Fig. 5, the aluminum alloy (A5052) specimen is a 100 mm × 100 mm × 50 mm rectangular solid having three side drilled holes (SDHs). The SDHs #1, #2, and #3 are located at 20 mm, 25 mm, and 30 mm from the upper surface, and at 20 mm, 40 mm, and 60 mm from the left surface, respectively. The diameter of # 1 and #3 are 3.0 mm, while diameter of #2 is 3.5 mm.

Waveforms were collected and processed in two different ways, PWI and FMC/TFM, respectively. For a PA probe having N elements, in PWI, all piezo elements excite the signals simultaneously and all the elements collect waveforms independently. Then $1 \times N$ waveforms are collected.

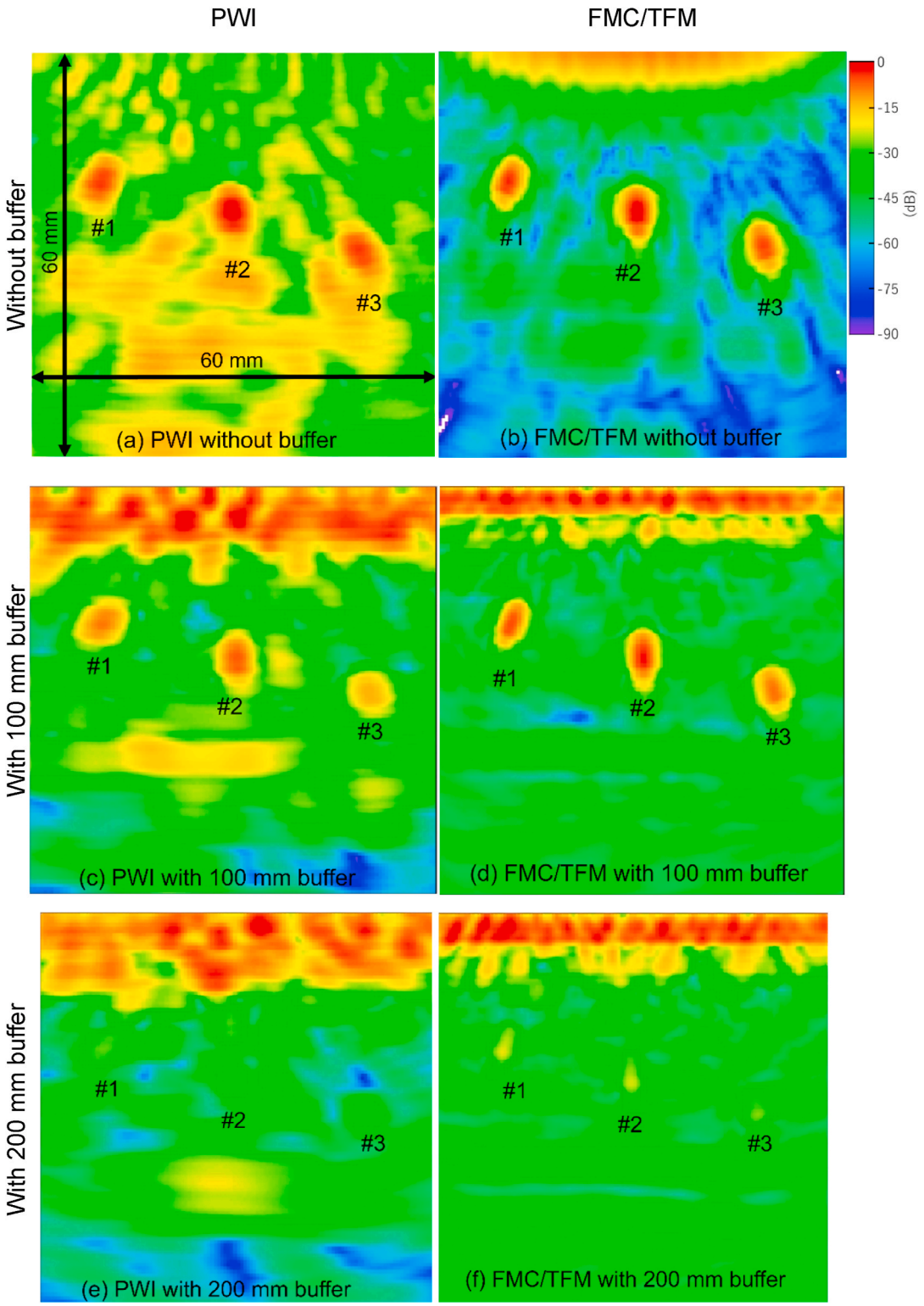

Fig. 7. Defect images when using the PA probe with and without the buffer consisting of a bundle of circular cylinders. (a) PWI without buffer. (b) FMC/TFM without buffer. (c) PWI with 100 mm buffer. (d) FMC/TFM with 100 mm buffer. (e) PWI with 200 mm buffer. (f) FMC/TFM with 200 mm buffer.

When using FMC/TFM, in each testing period, one element emits the signal and all the elements receive the echo from the specimen. This pulse emission from a single element and signal acquisition with all elements is performed repeatedly and then collect an $N \times N$ waveform set. Then the delay and sum processing based on the TFM are applied to the waveform set. Intensity of each specific position in the imaging area is calculated based on the expected delay.

Before the imaging experiment of the buffer consisting of a bundle of circular cylinders, the imaging experiment was performed with the PA probe without the buffer, as shown in Fig. 6 (a). After confirming that the defect image can be obtained with the PA probe, the imaging experiment was performed with the buffer consisting of a bundle of circular cylinders, as shown in Fig. 6 (b). During the experiments, a regular couplant for longitudinal waves was applied on the surface

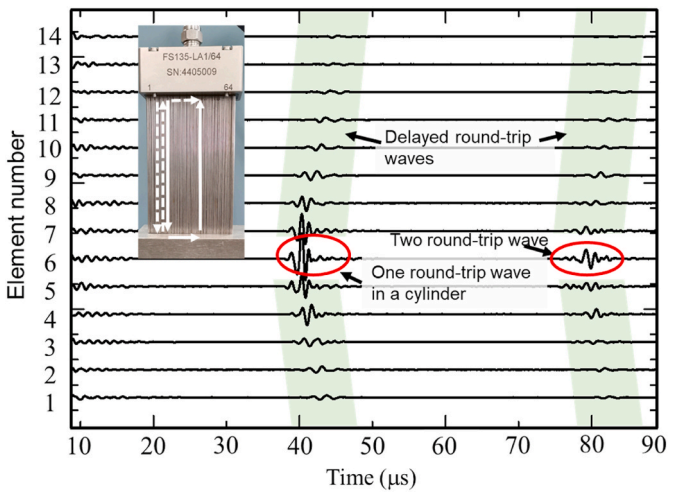

Fig. 8. Typical waveforms recorded in FMC. Element #6 is the incident element and the waveforms at the adjacent elements are shown.

between contact surfaces such as the PA probe and specimen, the PA probe and buffer, and the buffer and specimen. When performing actual inspections at high temperatures, an adhesive or couplant that can be applied at the expected high temperatures is required. The imaging area called regions of interest (ROI) in the latter experiments are rectangular of 60 mm × 60 mm (white square) and 60 mm × 130 mm (black dashed rectangular) as shown in the figure. The upper and lower edges of the buffer consisting of a bundle of circular cylinders are connected to the PA probe and upper surface of the specimen, respectively.

4. Results and discussions of experiments using buffer consisting of a bundle of circular cylinders

Fig. 7 shows the defect images using the PA probe with and without the buffer in two different ways as PWI and FMC/TFM. In the first row of the figure, (a) and (b), are images without buffer, and the second and third rows show the images with 100 mm and 200 mm long buffers, respectively. Columns denote the images for PWI and FMC/TFM. These imaging processes were done by assuming the guided waves of longitudinal mode propagates in the buffer with a group velocity of 5060 m/s, and longitudinal waves propagate with a velocity of 6200 m/s in the aluminum specimen used in the experiment. The colors of the images represent intensities expressed in a range from −90 to 0 dB, where the intensity values are normalized by the maximum intensity value of each figure.

In Fig. 7 (a) and (b) without a buffer, clear images of three SDHs were obtained at the correct positions and the images with FMC/TFM are clearer than those of PWI due to the difference of imaging algorithm. These images serve as a reference for comparison with conventional imaging using a PA probe. In Fig. 7(c) and (d), the SDH images are also clearly shown at the correct positions even with a buffer consisting of a bundle of circular cylinders, which indicates that the issues caused by trailing waves observed in the previous paper using a plate buffer [28] have been resolved as expected.

In Fig. 7 (e) and (f) with 200 mm long buffer, both for PWI and FMC/TFM, the intensity is lower at the defect positions, compared to (a) - (d), and defects cannot be recognized in (e), with PWI. There are several possible reasons for this degradation of the images; one is the attenuation of the guided waves in cylinders by using longer cylinders, the second one is the dispersion of the guided waves, and the third one is crosstalk between cylinders. At present, the third reason seems to be the dominant one, because the images were greatly distorted and defect images were not obtained when the coupling medium got into the gaps between the cylinders. Moreover, longer thin cylinders are also easy to

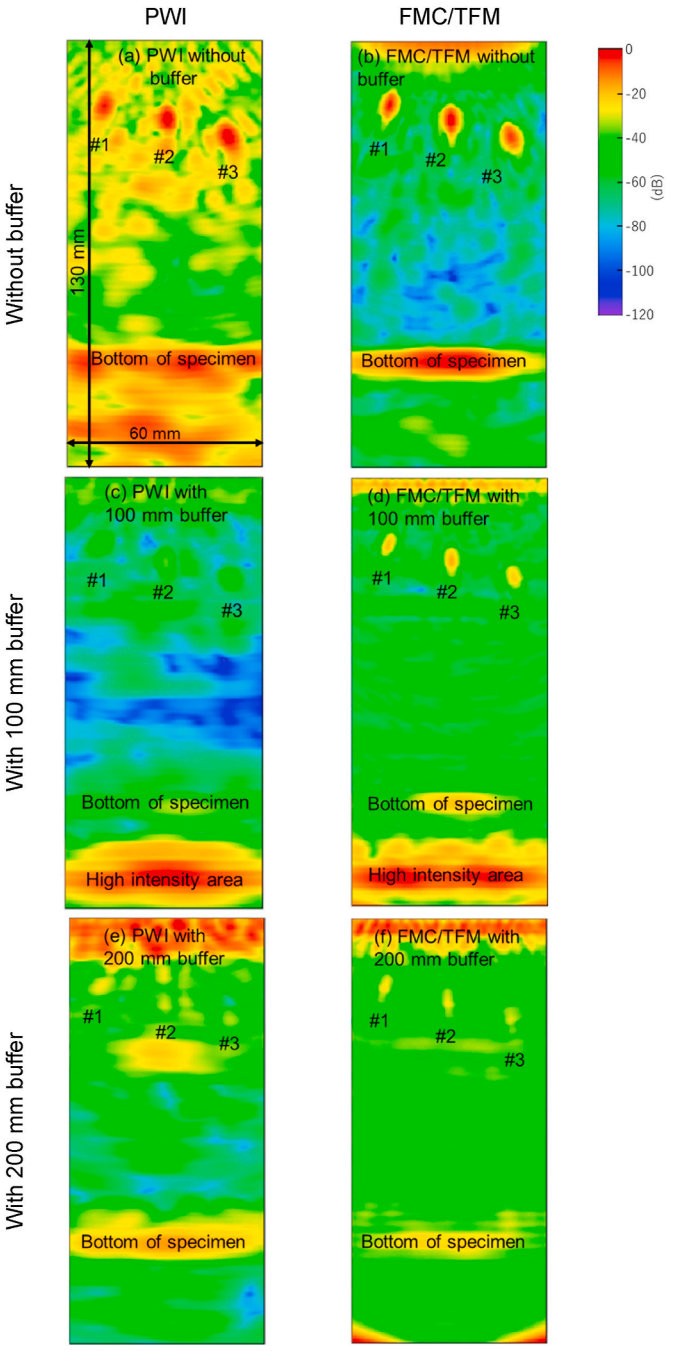

Fig. 9. Defect images when using the PA probe with and without the buffer consisting of a bundle of circular cylinders when the ROI is set to be 60 mm × 130 mm. (a) PWI without buffer. (b) FMC/TFM without buffer. (c) PWI with 100 mm buffer. (d) FMC/TFM with 100 mm buffer. (e) PWI with 200 mm buffer. (f) FMC/TFM with 200 mm buffer.

be bended and easy to be contacted with each other in which way cause the crosstalk between the cylinders. In the next fabrication of the circular cylinder buffers, we aim to create a buffer with minimal crosstalk by placing appropriately sized rigid balls with small contact areas in the gaps between the circular cylinders, thereby preventing cylinder contact and improving defect imaging.

Compared to (a) and (b), (c) – (f) have a high intensity area at the upper edge of the ROI indicating the echo noise generated at the interface between the buffer and the specimen, which leads to the lower intensity at the defect positions. To discuss this dead zone, Fig. 8 shows part of the waveforms used to obtain the images in Fig. 7. These are the

waveforms received by the first to 14th elements of the linear array probe when incident wave is generated only at the 6th element, at which a 100 mm buffer is attached. The wave packet at around 40 μs in the waveform received by the sixth element is the first reflected wave at the interface between the cylinder and the test specimen, and the wave packet at around 80 μs is two-round-trip wave in the cylinders of 6th row. Although only the sixth element is emitting the ultrasonic pulse, it can be seen in the neighboring elements that the one-round-trip wave and two-round-trip wave are received slightly later from the reflected waves received at 6th element. These delayed round-trip waves suggest the wave propagates in the buffer and specimen as follows; when the guided wave propagating through the sixth cylinder reaches the test specimen, it becomes not only a longitudinal wave propagating inside the test specimen but also interface waves propagating between the specimen surface and the buffer surface, which then propagates to the adjacent cylinder (solid arrow in Fig. 8). As the other propagation paths, the dashed arrows are also available. Namely, incident guided wave in the 6th cylinder reflects and propagates back in the same and/or the other cylinders, and then interface waves between the PA probe and the buffer surface reach the receiving elements. These delayed waves propagation partially at the interfaces are mixed in the receiving waveforms.

In the imaging using a buffer, the time of the one round-trip wave corresponds to the image of the interface between the buffer and the test specimen, and the subsequent time creates an image at the vicinity of the interface. Therefore, due to the influence of the slightly delayed round-trip wave propagated into the adjacent element, a high-intensity area, or dead zone, formed widely at the upper end of the ROI.

When using a buffer, imaging is performed using echoes from defects that appear between the first and second round-trip waves in the waveforms as shown in Fig. 8. Since the one and two round-trip waves appear very large, the echoes between them are invisible in the figure. In other words, when acquiring images, inclusion of the one and two round-trip waves significantly affects the results. In our previous study [27], we defined and theoretically and experimentally discussed the effective detecting region (EDR) that can be imaged only from the time range between the one and two round-trip waves, considering the velocity dispersion of guide waves in the buffer and the propagation of ultrasonic longitudinal waves in the test specimen, based on theoretical and experimental results.

Fig. 7 revealed that a long buffer cannot effectively acquire defect images due to the signal distortion, but a short buffer has the problem that the interval between the one and two round trips becomes shorter, resulting in a smaller EDR. Therefore, we discuss EDR by acquiring images of the bottom of the test specimen. Fig. 9 shows the images obtained when the imaging area was set to 60 mm × 130 mm using the same recorded waveform data as in Fig. 7. As in Fig. 9, the images using PWI and FMC/TFM, as well as those with no buffer, a 100 mm buffer, and a 200 mm buffer, are shown. The images are normalized using the maximum intensity value within each image, and the intensity values are displayed in color using a decibel scale from −120 to 0 dB. In the images without a buffer (a) and (b), in both cases, the defect images are accompanied by a large intensity value at the bottom surface of the test specimen, which is 100 mm away from the top surface where the PA probe is in contact. On the other hand, in cases (c) and (d) using a 100 mm buffer, a region with high intensity values appears below the bottom surface position. This is due to two round-trip waves that have traveled back and forth twice within the buffer, representing the limit region of EDR. Due to these regions, the image of the test specimen bottom becomes unclear. Conversely, in cases (e) and (f) where the buffer is extended to 200 mm, the high intensity areas disappear, making the image of the test specimen bottom clearer. As such, it was also demonstrated, while using a longer buffer tends to result in image blurring due to crosstalk, as seen in Fig. 7, this has the beneficial effect of expanding the EDR.

5. Conclusion

Defect imaging using a PA probe attached with a buffer consisting of a bundle of circular cylinders was proposed and its feasibility was experimentally investigated. A circular cylinder with a diameter of 0.9 mm was used as a waveguide to transmit ultrasonic waves output from each vibrating element of a PA probe. This was determined by considering the width of the vibrating element of the PA probe and the characteristics of the guided wave longitudinal vibration mode propagating in the waveguide. Experiments were conducted to image the SDH and bottom surface of an aluminum block using buffers with lengths of 100 mm and 200 mm, fabricated by arranging the circular cylinders. The results showed that the shorter 100 mm buffer produced clearer images due to factors such as guided wave attenuation, dispersion, and crosstalk between the circular cylinders. On the other hand, it was also confirmed that the effective detecting region narrowed when using the shorter buffer. Additionally, delayed reflected waves were observed, where the waves emitted from the circular cylinders propagated as Rayleigh waves on the test specimen surface and transmit into other cylinders, thereby enlarging the dead zone near the test specimen surface.

This technology is expected to be used for imaging objects that cannot be directly contacted with a PA probe, such as those at high or extremely low temperatures.

CRediT authorship contribution statement

Mingqian Xia: Writing – review & editing, Writing – original draft, Validation, Methodology, Investigation, Data curation. **Kohei Nishiuchi:** Writing – original draft, Methodology, Investigation, Data curation. **Takahiro Hayashi:** Writing – review & editing, Writing – original draft, Supervision, Project administration, Methodology, Investigation, Funding acquisition, Data curation. **Naoki Mori:** Writing – review & editing, Writing – original draft, Validation, Methodology, Investigation, Conceptualization.

Declaration of competing interest

The authors declare the following financial interests/personal relationships which may be considered as potential competing interests: Takahiro Hayashi reports financial support and administrative support were provided by Japan Atomic Energy Agency. If there are other authors, they declare that they have no known competing financial interests or personal relationships that could have appeared to influence the work reported in this paper.

Acknowledgements

This word was supported by JAEA Nuclear Energy S&T and Human Resource Development Project through concentrating wisdom Grant Number JPJA 24P2420343.

Data availability

Data will be made available on request.

References

[1] Alleyne DN, Pavlakovic B, Lowe MJS, Cawley P. Rapid, long range inspection of chemical plant pipework using guided waves. AIP Conf Proc 2001;557:180–7. https://doi.org/10.1063/1.1373757.
[2] Morgan BC, Tilley R. Inspection of power plant headers utilizing acoustic emission monitoring. NDT E Int 1999;32(3):167–75. https://doi.org/10.1016/S0963-8695(98)00068-1.
[3] Ma J, Jiang J. Applications of fault detection and diagnosis methods in nuclear power plants: a review. Prog Nucl Energy 2011;53(3):255–66. https://doi.org/10.1016/j.pnucene.2010.12.001.
[4] Oh S, Yun DS, Kim J. Evaluation of high-temperature degradation of platen superheater tube in thermoelectric power plant using nonlinear surface ultrasonic

waves. Ultrasonics 2024;136:107162. https://doi.org/10.1016/j.ultras.2023.107162.
[5] Sposito G, Ward C, Cawley C, Nagy PB, Scruby C. A review of non-destructive techniques for the detection of creep damage in power plant steels. NDT E Int 2010;43(7):555–67. https://doi.org/10.1016/j.ndteint.2010.05.012.
[6] Takaya S, Miya K. Application of magnetic phenomena to analysis of stress corrosion cracking in welded part of stainless steel. J Manuf Process 2005;161:66–74. https://doi.org/10.1016/j.jmatprotec.2004.07.017.
[7] Fan E, Li Y, Lv X. A study on the stress corrosion mechanism of microstructures in a heat-affected zone of high-strength steel weldment in artificial seawater. Surf Topogr Metrol Prop 2021;9:025040.
[8] Sugawara A, Jinno K, Ohara Y, Yamanaka K. Closed-crack imaging and scattering behavior analysis using confocal subharmonic phased array. Jpn J Appl Phys 2015;54:07HC08. https://doi.org/10.7567/JJAP.54.07HC08.
[9] Khodamorad SH, Alinezhad N, Haghshenas Fatmehsari D, Ghahtan K. Stress corrosion cracking in Type.316 plates of a heat exchanger. Case Stud Eng Fail Anal 2016;5–6:59–66. https://doi.org/10.1016/j.csefa.2016.03.001.
[10] Yu L, Liu Y, Deng H, Zhang S, Wang Y, Zhou Y. Cracking failure analysis of pipe to flange weld joint. IOP Conf Ser Earth Environ Sci 2021;859:012012. https://doi.org/10.1088/1755-1315/859/1/012012.
[11] Suleimanov RI, Zainagalina LZ, Khabibullin MY, Zaripova LM, Kovalev NO. Studying heat-affected zone deformations of electric arc welding. IOP Conf Ser Mater Sci Eng 2018;327:032053. https://doi.org/10.1088/1757-899X/327/3/032053.
[12] Vasilev M, MacLeod C, Galbraith W, Javadi Y, Foster E, Dobie G, Pierce G, Gachagan A. Non-contact in-process ultrasonic screening of thin fusion welded joints. J Manuf Process 2021;64:445–54. https://doi.org/10.1016/j.jmapro.2021.01.033.
[13] Li Q, Chen Y, Tang Y, Liu H. Ultrasonic phased array detection method for butt fusion welding defects of HDPE pipes. J Phys: Conf Ser 2023;2419:012071. https://doi.org/10.1088/1742-6596/2419/1/012071.
[14] Ohara Y, Yamamoto S, Mihara T, Yamanaka K. Ultrasonic evaluation of closed cracks using subharmonic phased array. Jpn J Appl Phys 2008;47:3908. https://doi.org/10.1143/JJAP.47.3908.
[15] Ohara Y, Potter J, Nakajima H, Tsuji T, Mihara T. Multi-mode nonlinear ultrasonic phased array for imaging closed cracks. Jpn J Appl Phys 2019;58:SGGB06. https://doi.org/10.7567/1347-4065/ab0adc.
[16] Ohara Y, Nakajima H, Haupert S, Tsuji T, Mihara T. Imaging of three-dimensional crack open/closed distribution by nonlinear ultrasonic phased array based on fundamental wave amplitude difference. Jpn J Appl Phys 2020;59:SKKB01. https://doi.org/10.35848/1347-4065/ab79ea.
[17] Wu Y, Wilcox PD, Croxford AJ. Fastener hole inspection using 2D phased array. NDT E Int 2024;143:103057. https://doi.org/10.1016/j.ndteint.2024.103057.
[18] Xu N, Zhou Z. Numerical simulation and experiment for inspection of cornershaped components using ultrasonic phased array. NDT E Int 2014;63:28–34. https://doi.org/10.1016/j.ndteint.2014.01.005.
[19] Sumana Kumar A. Phased array ultrasonic imaging using angle beam virtual source full matrix capture-total focusing method. NDT E Int 2020;116:102324. https://doi.org/10.1016/j.ndteint.2020.102324.
[20] Hampson R, Zhang D, Gachagan A, Dobie G. Modelling and characterisation ultrasonic phased array transducers for pipe inspections. Int J Pres Ves Pip 2022;200:104808. https://doi.org/10.1016/j.ijpvp.2022.104808.
[21] Nicolson E, Mohseni E, Lines D, Tant KMM, Pierce G, MacLeod CN. Towards an inprocess ultrasonic phased array inspection method for narrow-gap welds. NDT E Int 2024;144:103074. https://doi.org/10.1016/j.ndteint.2024.103074.
[22] Dupont-Marillia F, Jahazia M, Lafreniereb S, Belangera P. Design and optimisation of a phased array transducer for ultrasonic inspection of large forged steel ingots. NDT E Int 2019;103:119–29. https://doi.org/10.1016/j.ndteint.2019.02.007.
[23] Foudzi FM, Ihara I. Development of polygonal buffer rods for ultrasonic pulse-echo measurements. J Phys: Conf Ser 2014;520:012025. https://doi.org/10.1088/1742-6596/520/1/012025.
[24] Ihara T, Tsuzuki N, Kikura H. Development of the ultrasonic buffer rod for the molten glass measurement. Prog Nucl Energy 2015;82:176–83. https://doi.org/10.1016/j.pnucene.2014.07.041.
[25] Kazys R, Vaskeliene V. High temperature ultrasonic transducers: a review. Sensors 2021;21:3200. https://doi.org/10.3390/s21093200.
[26] Fukuchi T, Hayashi T, Mori N. Ultrasonic focusing using a stacked thin-plate region. Jpn J Appl Phys 2023;62:SJ1005. https://doi.org/10.35848/1347-4065/acb361.
[27] Xia M, Hayashi T, Mori N. Numerical analysis of the phased array imaging with a stacked plate buffer. Jpn J Appl Phys 2024;63:03SP55. https://doi.org/10.35848/1347-4065/ad25a9.
[28] Xia M, Hayashi T, Mori N. Experimental investigation of defect imaging using a phased array probe with a stacked plate buffer. NDT E Int 2025;151:103316.
[29] Redwood M. Narrow-bandwidth pulses in solid waveguides. Mechanical waveguides. New York: Pergamon Press; 1960. p. 190–207.
[30] Hayashi T, Song W, Rose JL. Guided wave dispersion curves for a bar with an arbitrary cross-section, a rod and rail example. Ultrasonics 2003;41:175–83.